AD-750 359

A THEORETICAL AND EXPERIMENTAL INVESTIGATION OF FLAP--LAG STABILITY OF HINGELESS HELICOPTER ROTOR BLADES

Robert A. Ormiston, et al

Army Air Mobility Research and Development Laboratory
Moffett Field, California

1972

DISTRIBUTED BY:

NTIS

National Technical Information Service
U. S. DEPARTMENT OF COMMERCE
5285 Port Royal Road, Springfield Va. 22151

DISCLAIMER NOTICE

THIS DOCUMENT IS BEST QUALITY PRACTICABLE. THE COPY FURNISHED TO DTIC CONTAINED A SIGNIFICANT NUMBER OF PAGES WHICH DO NOT REPRODUCE LEGIBLY.

145

AD 750 359

AD750359

A THEORETICAL AND EXPERIMENTAL INVESTIGATION OF FLAP-LAG STABILITY OF HINGELESS HELICOPTER ROTOR BLADES

Robert A. Ormiston and William G. Bousman
Ames Directorate
U. S. Army Air Mobility Research & Development Laboratory
Moffett Field, CA 94035

DDC

INTRODUCTION

The hingeless rotor has become an attractive concept for conventional and compound helicopters in recent years. The primary reasons for this attractiveness lie in the anticipation that the increased control power and angular damping of the hingeless rotor will greatly enhance flying qualities and maneuverability, and the simpler hub design will result in reduced maintenance and improved reliability. The AH-56A Cheyenne is an example of a compound helicopter using a hingeless rotor and it is likely that at least one of the UTTAS candidate aircraft will have a hingeless rotor. Unfortunately, experience with the AH-56A has revealed a number of unpredicted and potentially catastrophic rotor blade instabilities. These instabilities were not previously encountered with conventional articulated rotor helicopters, and can be attributed largely to the paucity of basic research on hingeless rotors. Until their fundamental dynamic stability characteristics are thoroughly understood, the promise of the hingeless rotor for advanced rotary wing aircraft will not be fulfilled.

A substantial insight into the fundamental stability characteristics of the hingeless rotor may be obtained by considering only the flap and lead-lag degrees of freedom of a single blade. Although portions of this problem have been examined in previous research, the effects of many basic rotor parameters are poorly understood. The present study therefore was undertaken to provide a rigorous formulation of the problem, and to systematically investigate the important parameters which characterize actual hingeless rotor blade configurations. In the absence of available experimental data a model rotor was designed and tested to validate the theoretical analysis. As a result of these investigations several practical approaches can now be suggested for improving the inherent stability of hingeless rotor blades.

Reproduced by
NATIONAL TECHNICAL
INFORMATION SERVICE
U S Department of Commerce
Springfield VA 22151

Begin → 115

14

6

THEORETICAL ANALYSIS

Equations of Motion

The basic flap and lead-lag deflections of a hingeless rotor blade are measured with respect to an x, y, z, coordinate system positioned in the undeformed blade and rotating with angular velocity Ω, Fig. 1. The axis of rotation is fixed in space and for simplicity the blades are considered rigid in torsion. The problem is restricted to hover in order to eliminate periodic coefficients in the equations of motion. Although the motion of the elastically deflected rotor blade in Fig. 1 must be described by partial differential equations, considerable simplification can be obtained by replacing the elastic blade with an appropriately hinged rigid blade where spring elements are used to simulate the elastic properties of the actual rotor blade, Fig. 2. The problem is then simplified to one involving only ordinary differential equations* which in turn greatly enhances the physical insight provided by the theory.

An important feature of hingeless rotor blades is that when the collective pitch angle changes, the elastic principle axes of the portion of the blade outboard of the pitch bearing also rotate, thus altering the relative stiffnesses in the flapping and lead-lag directions. Furthermore, this rotation couples these degrees of freedom elastically, that is, flap deflections produce lead-lag bending moments and vice-versa. The degree of this elastic coupling is strongly dependent on the radial position of the pitch change bearing, Fig. 1, or in other words the relative blade flexibility occurring inboard and outboard of the pitch bearing.

The importance of this coupling requires that the flap and lead-lag hinge springs of the rigid blade be divided into two distinct orthogonal systems -- one located inboard and one outboard of the pitch bearing, as shown in Fig. 2. The degree of elastic coupling is determined by the relative flexibilities of the two spring systems.

Although the pitch bearing location is an important design parameter for hingeless rotor helicopters the associated elastic coupling effects have not been included in previous studies of rotor blade stability nor have they been recognized as a significant factor in flap-lag stability.

The differential equations of motion for the flap and lead-lag angular deflections (β,ζ) for the rigid blade representation of the hingeless rotor are obtained by summing the flap and lead-lag moments due to aerodynamic, inertial, and elastic forces. A complete derivation is given in Ref. 1. Since the equations are nonlinear, it is advantageous to consider the stability of small deflections from the equilibrium condition. The equations for the flap and lead-lag perturbation deflections ($\Delta\beta$, $\Delta\zeta$) are thereby linearized. First, the equations for the equilibrium deflections (β_o, ζ_o) are

*The exact partial differential equations have been developed and compared with the present approximate equations in Ref. 1. The results indicate a high degree of accuracy for the approximate equations.

$$\begin{bmatrix} p^2 & z^2 \\ z^2 & q^2 \end{bmatrix} \begin{Bmatrix} \beta_o \\ \zeta_o \end{Bmatrix} = \gamma/8 \begin{Bmatrix} \theta - A \\ -\left(\frac{c_{d_o}}{a} + A\theta - C\right) \end{Bmatrix} \tag{1}$$

After taking the Laplace transform, the perturbation equations become,

$$\begin{bmatrix} s^2 + \frac{\gamma}{8} s + p^2 & -s\left[\frac{\gamma}{8}(2\theta - A) - 2\beta_o\right] + z^2 \\ -s\left[2\beta_o - \frac{\gamma}{8}(\theta - 2A)\right] + z^2 & s^2 + s\frac{\gamma}{8}\left(2\frac{c_{d_o}}{a} + A\theta + \frac{16\eta_m \bar{\omega}_\zeta}{\gamma}\right) + q^2 \end{bmatrix} \begin{Bmatrix} \Delta\beta \\ \Delta\zeta \end{Bmatrix}$$

$$= \Delta\theta \left[\frac{\gamma}{8} \begin{Bmatrix} 1 \\ -A \end{Bmatrix} - R\frac{(\bar{\omega}_\zeta^2 - \bar{\omega}_\beta^2)}{\Delta} \left\{ R_w \begin{bmatrix} [\beta_o - \frac{\gamma}{8}(\theta - A)] \\ \frac{\gamma}{8}\left(\frac{c_{d_o}}{a} + A\theta - C\right) \end{bmatrix} + \beta_o \begin{bmatrix} \sin 2\theta \\ \cos 2\theta \end{bmatrix} + \zeta_o \begin{bmatrix} \cos 2\theta \\ -\sin 2\theta \end{bmatrix} \right\} \right] \tag{2}$$

where

$$p^2 = 1 + \frac{1}{\Delta}\left[\bar{\omega}_\beta^2 + R(\bar{\omega}_\zeta^2 - \bar{\omega}_\beta^2)\sin^2\theta\right] \tag{3}$$

$$q^2 = \frac{1}{\Delta}\left[\bar{\omega}_\zeta^2 - R(\bar{\omega}_\zeta^2 - \bar{\omega}_\beta^2)\sin^2\theta\right] \tag{4}$$

$$z^2 = \frac{R}{2\Delta}(\bar{\omega}_\zeta^2 - \bar{\omega}_\beta^2)\sin 2\theta \tag{5}$$

$$\Delta = 1 + R(1-R)\frac{[\bar{\omega}_\zeta^2 - \bar{\omega}_\beta^2]^2}{\bar{\omega}_\zeta^2\bar{\omega}_\beta^2}\sin^2\theta \quad , \qquad R_w = (1-R)\frac{[\bar{\omega}_\zeta^2 - \bar{\omega}_\beta^2]}{\bar{\omega}_\zeta^2\bar{\omega}_\beta^2}\sin 2\theta \tag{6}$$

$$\bar{\omega}_\beta^2 = K_\beta/I\Omega^2 \quad , \qquad \bar{\omega}_\zeta^2 = K_\zeta/I\Omega^2 \tag{7}$$

$$K_\beta = \frac{K_{\beta_B} K_{\beta_H}}{K_{\beta_B} + K_{\beta_H}} \quad , \quad K_\zeta = \frac{K_{\zeta_B} K_{\zeta_H}}{K_{\zeta_B} + K_{\zeta_H}} \tag{8}$$

$$R = K_\beta / K_{\beta_B} = K_\zeta / K_{\zeta_B} \tag{9}$$

The terms associated with aerodynamic forces are the Lock number γ, profile drag coefficient c_{d_o}, lift curve slope a, and the induced inflow parameters A, C which are approximated using momentum theory, Ref. 2.

$$A = \frac{a\sigma}{12}\left[\sqrt{1 + \frac{24\theta}{a\sigma}} - 1\right] \quad , \quad C = A^2 \tag{10}$$

The collective pitch angle is given by θ. The Coriolis and centrifugal inertial forces arise from the equilibrium flap deflection or coning, β_o. The remaining terms involve elastic forces which are unique to the hingeless rotor. The non-rotating flap and lead-lag frequencies $\bar{\omega}_\beta$ and $\bar{\omega}_\zeta$ broadly define various classes of hingeless rotor blade configurations. For instance soft inplane rotors are characterized by $\bar{\omega}_\zeta < 1.0$* and stiff inplane rotors by $\bar{\omega}_\zeta > 1.0$**. The parameter R is used to define the degree of elastic coupling. For R = 0.0, the blade flexibility is located inboard of the pitch bearing and no elastic coupling is introduced as pitch angle is increased from zero. The converse is true for R = 1.0 and intermediate values of R define varying degrees of elastic coupling.

The small perturbation stability of flap and lead-lag motions defined by these equations will be examined for three distinct cases: 1) basic flap-lag coupling (R = 0.0), 2) the effects of variable elastic coupling (R ≠ 0.0), and 3) the influence of kinematic pitch-lag coupling.

Basic Flap-Lag Stability

The homogeneous portion of Eq. (2) governs the basic flap-lag stability of hingeless rotors. For R = 0.0, the only coupling between the flap and lead-lag degrees of freedom is due to aerodynamic and inertial forces, the single underlined terms in Eq. (2). The damping in the lead-lag equation is inherently very small since it consists of only profile drag damping, induced inflow damping, and structural damping ($\frac{16\eta_m\bar{\omega}_\zeta}{\gamma}$). Under certain conditions, the product of the basic aerodynamic and inertial flap-lag coupling terms is destabilizing and may provoke an instability of the weakly damped lead-lag mode. This is shown in Fig. 3 which is a locus of roots of the flap-lag characteristic equation plotted in the complex plane. The locus for several configurations ($\bar{\omega}_\zeta$ = 0.7, 0.9, 1.10,

* i.e., the Bolkow BO-105, $\bar{\omega}_\zeta \approx 0.7$

** i.e., the Lockheed AH-56A Cheyenne, $\bar{\omega}_\zeta \approx 1.4 - 1.6$

1.15, 1.20, 1.40) traces the roots as collective pitch is increased from 0.0 to 0.5 rad. When $\bar{\omega}_\zeta$ is close to the rotating flap frequency ($p = \sqrt{4/3} = 1.1547$), the lead-lag mode becomes unstable.

Although the unstable configurations do not represent typical designs (other constraints preclude the $\bar{\omega}_\zeta \approx p$ configuration) these results do afford new insight into the physical mechanisms which govern the stability of hingeless rotor blades. For instance, Routh's criterion for the neutral stability condition can be used to derive a formula for the lowest collective pitch angle at which the rotor blade becomes unstable. Thus we have

$$(\theta-A)^2 = \frac{P^2}{2(P-1)(2-P)}\left\{D + \frac{(D+A\theta)(P-W)^2}{(\gamma/8)^2[W+P(D+A\theta)](1+D+A\theta)}\right\} \tag{11}$$

where

$$D = 2\left[\frac{c_{d_o}}{a} + \frac{8\eta_m\bar{\omega}_\zeta}{\gamma}\right] \quad ; \quad P = p^2 \quad ; \quad W = \bar{\omega}_\zeta^2 \tag{12}$$

Since $D \geq 0$ and $A\theta \geq 0$, it follows that a necessary (but not sufficient) condition for instability is that $1 < p^2 < 2$. This indicates that simple articulated rotors cannot be unstable since $p = 1$. In addition, for a given flapping frequency, p, the minimum collective pitch for neutral stability, θ_{min}, occurs when $\bar{\omega}_\zeta = p$.

$$(\theta_{min}-A)^2 = \frac{P^2 D}{2(P-1)(2-P)} \tag{13}$$

For $p = \sqrt{4/3}$ an absolute minimum occurs in the collective pitch for neutral stability. This value, referred to as θ^* is

$$(\theta^*-A)^2 = 4D = 8\left[\frac{c_{d_o}}{a} + \frac{16\sqrt{3}}{3}\frac{\eta_m}{\gamma}\right] \tag{14}$$

These simple and concise relations clearly show the dependence of flap-lag stability on the basic system parameters and design variables.

Both profile drag and structural damping are stabilizing, as is the induced inflow represented by the parameter A. Since induced inflow increases with rotor solidity, σ, increased blade chord or number of blades is stabilizing. When $p \neq \bar{\omega}_\zeta$ the stability depends on the combination of p and $\bar{\omega}_\zeta$, together with the Lock number. This dependency is shown in Fig. 4, which maps the neutral stability boundaries as a function of flap and lead-lag frequencies. For a particular collective pitch the region of instability lies within the respective contour. These results illustrate the occurrence of θ_{min} for a given value of p when $\bar{\omega}_\zeta = p$, and θ^* when $p = \sqrt{4/3}$ as indicated by Eqs. (13) and (14).

Effect of Variable Elastic Coupling

The elastic flap-lag coupling terms are doubly underlined in Eq. (2). They are roughly proportional to the collective pitch angle, the elastic coupling parameter R, and the difference between the flap and lead-lag nonrotating frequencies ($\bar{\omega}_\zeta^2 - \bar{\omega}_\beta^2$). The

importance of these terms for hingeless rotor blades is immediately apparent by comparing the locus of roots with elastic coupling in Fig. 5 with the previous case, Fig. 3. Only three lead-lag frequencies are shown, which typify practical soft-inplane $\bar{\omega}_\zeta = .7$ and stiff-inplane $\bar{\omega}_\zeta = 1.4$ rotor blade configurations. The third case, $\bar{\omega}_\zeta = 1.1$, is included for comparison. The stiff inplane rotor blade is highly unstable for small values of R, while the lead-lag damping of the soft inplane rotor blade is increased. Values of R near 1.0 are highly stabilizing in both cases, particularly for the stiff inplane configuration. Stability boundaries as a function of lead-lag frequency and elastic coupling are shown in Fig. 6. This plot illustrates that the minimum pitch angle for instability is determined by a specific relationship between the lead-lag frequency and R.

Routh's criterion may again be used to investigate this case. For small pitch angles ($\theta^2 << 1$) the pitch angle for neutral stability is given by

$$(\theta-A)^2 = \frac{p^2}{2(P-1)(2-P)}\left\{ D + \frac{\left[D - \frac{(\theta-A)^2}{4}\right](W-P)^2 + \left[\frac{(\theta+A)(W-P)}{2} - R\theta(W-P+1)\right]^2}{\eta^2 W}\right\} \quad (15)$$

Since $0 \leq R \leq 1$, elastic coupling can only be destabilizing when $W > P$ or $W < P - 1$. This explains why only stiff inplane rotor blades become unstable in Figs. 5 and 6. When $p = \sqrt{4/3}$, the value of R corresponding to the least stable value of lead-lag frequency may be obtained from the following relation.

$$R = \frac{\theta^*+A}{2\theta^*} \frac{(\bar{\omega}_\zeta^2 - 4/3)}{(\bar{\omega}_\zeta^2 - 1/3)} \quad (16)$$

It is of interest that the pitch angle for this condition is precisely that given by Eq. (15) for basic flap-lag instability, i.e., θ^*, which explains why the minimum pitch angle for instability in Fig. 6 was independent of R and $\bar{\omega}_\zeta$.

The practical importance of elastic coupling is that while small values of R are potentially dangerous for stiff inplane rotor blades, large values of R provide a means of greatly increasing the inherently weak lead-lag damping of both soft and stiff inplane rotor blades. In the present state of the art of hingeless rotor design, no sound rationale exists regarding the influence of pitch bearing location and elastic coupling on rotor blade stability characteristics. Present design philosophy is largely based on intuitive tradeoffs between blade stresses, bending torsion coupling, and rotor control power. Therefore, the present analysis could provide a basis for a rational approach toward eliminating hingeless rotor instabilities.

Pitch-Lag Coupling

Coupling between the blade pitch angle and the lead-lag deflection can be caused by either control system kinematics or coupled bending-torsion of the rotor blade. The former effect is a well known cause of articulated rotor instability. However, both factors are significant for hingeless rotors and are not yet well understood. The present perturbation flap-lag equations including the nonhomogeneous terms may be used to investigate this subject. The necessary equation for pitch-lag coupling is given by $\Delta\theta = \theta_\zeta \Delta\zeta$ where θ_ζ is the magnitude of the coupling. In particular the combined effects of elastic coupling and pitch lag coupling will be examined. The results are given in the form of stability boundaries for a soft and a stiff inplane configuration in Fig. 7. For the soft inplane ($\bar{\omega}_\zeta = .7$) case, the result is similar to an articulated rotor, positive θ_ζ is destabilizing, and the effect of variable elastic coupling is found to be slight. The stiff inplane configuration ($\bar{\omega}_\zeta = 1.4$), however, exhibits entirely different behavior. With no elastic coupling, negative θ_ζ produces instability. Elastic coupling, however, is strongly stabilizing for negative θ_ζ, but becomes progressively destabilizing as R increases and θ_ζ becomes positive. Therefore, potential instabilities exist for several combinations of pitch-lag coupling and elastic coupling. These results further emphasize the need for a rational approach to hingeless rotor design if instabilities arising from complex coupling effects are to be avoided.

EXPERIMENT

The theory discussed above shows that flap-lag coupling can destabilize rotor blade lead-lag oscillations. As previous experimental work to support this conclusion is absent, an experimental model was designed and tested to determine if the reduction in damping predicted by the basic flap-lag theory did indeed occur for a real system. To accomplish this validation it was necessary that the experimental model reproduce the theoretical model as closely as possible. In addition, it was necessary that the hinge stiffnesses be chosen so that the region of minimum stability could be examined.

Experimental Design

A sketch of the model hub is shown in Fig. 8. Flapping and lead-lag flexibility is contained in separate flexures, located as close to the hub centerline as possible. The hub and blade are designed for maximum stiffness outboard of the flexure. This design closely approximates the theoretical representation of a centrally-hinged, rigid blade with spring restraint. The only damping in the model hub is the structural damping in the flexures. The blade pitch angle is changed outboard of the flexures to avoid elastic coupling of flapping and lead-lag motions as pitch angle is changed. Torsional stiffness is provided by the flap flexures. The resulting torsional natural frequency is approximately twenty times as large

as either the flapping or lead-lag natural frequencies, which effectively decouples the torsional degree of freedom. The flapping stiffness, K_β, and lead-lag stiffness, K_ζ, were selected so that the region of minimum stability could be penetrated. Fig. 4 shows this region as a function of nondimensional flapping and lead-lag frequencies, where

$$p = \sqrt{1 + \frac{K_\beta}{I\Omega^2}} \quad ; \quad \bar{\omega}_\zeta = \sqrt{\frac{K_\zeta}{I\Omega^2}} \tag{17}$$

By simply varying the rotor speed, Ω, it was possible to change p and $\bar{\omega}_\zeta$ simultaneously, and thereby traverse the region of minimum stability. The blades were made of balsa wood with an aluminum spar. The major rotor parameters are

Lock number , γ	2.525
solidity , σ	0.0602
radius , R	2.97 feet
blade chord , c	0.281 feet
thickness ratio	12%
twist	-0.3035 deg/in
Reynolds number	$1.0 - 2.5 \times 10^5$

The hub and blades were mounted on a rigid test stand as shown in Fig. 9, and driven by an air motor. To measure damping of the lead-lag motions, the rotor was excited with an electrodynamic shaker in the nonrotating system, and the transient decay of the blade lead-lag oscillations was recorded after turning the shaker off.

Instrumentation

The blade root flexures were instrumented with strain gages to measure the flapping and lead-lag bending moments of both blades. In addition, the flap flexures on one blade were strain gaged to measure torsion moments. All gages were calibrated with applied moments so that angular deflection could be related directly to strain. The strain gage signals were removed from the rotating system with a forty channel set of slip rings (Fig. 9). The rotor speed was determined with an inductive pickup. Stand accelerations were determined with an accelerometer mounted below the hub. All output signals were recorded on an oscillograph and magnetic tape (for subsequent data processing), and an oscilloscope was used to monitor significant parameters.

Nonrotating Tests

Nonrotating tests were run to determine rotor stiffness and inertia characteristics. With the rotor hub locked to prevent rotation, flapping and lead-lag motions were excited separately for each blade (opposing blade removed), and their natural frequencies of oscillation were measured. In repeating these tests over a range of pitch angles from -2 degrees to 90 degrees, a small variation in the flapping and lead-lag natural frequencies was discovered as the pitch angle increased (Fig. 10). This variation results

because the rotor blade is not perfectly rigid outboard of the pitch change bearing, and therefore the flapping and lead-lag motions are elastically coupled. The degree of elastic coupling, R, can be determined from any three experimental points. Using this value and the theoretical model for elastic coupling, the predicted frequency variation is as shown in Fig. 10.

The structural damping of the lead-lag oscillations was measured, and was invariant for $0° \leq \theta_{.75R} \leq 18°$. The structural damping is 0.11% critical damping.

Rotating Tests

Rotating tests were run in order to examine both steady state and transient operation. Steady values of blade coning and profile drag coefficient were measured to compare with theoretical predictions, and to estimate the limits of linearized theory. Fig. 11 shows the steady coning as a function of collective pitch, where the coning angle has been normalized to remove the effect of rotor speed. The coning angle significantly departs from linear theory as the blade enters a stalled condition for collective pitch angles in the range of 12 to 14 degrees. Blade stall was observed experimentally in this region using wool tufts under stroboscopic lighting for flow visualization. This low stall angle is due to the low Reynolds number, and is predicted reasonably well by two-dimensional airfoil data, Ref. 3. As blade coning determines the extent of inertial flap-lag coupling, it is expected that the theory will overpredict the coupling effects at collective pitch angles above stall.

The mean profile drag coefficient calculated from the steady data is shown in Fig. 12. The two-dimensional drag coefficient data of Ref. 3 is shown for comparison. The damping of the lead-lag motions is strongly dependent upon the mean profile drag coefficient, which is assumed to have a constant value in the linear theory. For higher collective pitch angles it is expected that the linear theory will underestimate the amount of drag damping present.

The transient motion of the rotor blades during rotating tests was investigated by exciting the fixed hub in a direction parallel to the plane of rotation with an electrodynamic shaker at a frequency of $\Omega + \omega_\zeta$. In the rotating system, this excitation occurred at the lead-lag natural frequency, ω_ζ. When the lead-lag oscillatory amplitude was sufficiently large, excitation was terminated and the damped transient motion of the oscillations were recorded on the oscillograph and magnetic tape record. Measurements of lead-lag damping were made over a range of collective pitch angles and blade natural frequencies. Figure 13 shows the experimental nondimensional damping as a function of nondimensional lead-lag natural frequency for a collective pitch angle of 11.95 degrees. The theory without flap-lag coupling simply shows the effects of structural, profile, and induced drag damping which increase the lead-lag damping as the pitch angle is increased. The effect of flap-lag coupling, however, is to significantly reduce the damping for nondimensional lead-lag natural frequencies near the flapping

frequency. The experimental data confirm the predicted reduction due to aerodynamic and inertial flap-lag coupling. The effect of the small degree of elastic coupling is to shift the lead-lag frequency for minimum damping away from the frequency where $p = \bar{\omega}_\zeta$. The scatter in damping values at each lead-lag frequency is indicative of the difficulty in measuring very small values of damping (less than 0.4% critical damping). For $\bar{\omega}_\zeta$ 1.2, the test stand was not sufficiently rigid and its natural frequency coupled with the blade lead-lag motion to augment the lead-lag damping.

Figure 14 compares the experimental and theoretical lead-lag damping as a function of collective pitch angle for $\bar{\omega}_\zeta = 1.278$. This is the approximate frequency for minimum stability. The theory without flap-lag coupling shows a steady increase in damping with collective pitch and does not correlate with the measured data. The linear flap-lag theory, however, correctly predicts the decrease in damping that occurs as collective pitch is increased to the stall angle. Beyond stall the linear flap-lag theory continues to predict a reduction in the lead-lag stability, however, if modified to include the experimentally determined profile drag coefficient, the theory then correctly shows the strongly stabilizing effect of the profile drag damping of the stalled rotor. The data in Fig. 14 clearly confirm the necessity of including the flap-lag coupling terms in order to predict rotor blade stability.

Concluding Remarks

Several general conclusions may be summarized from these results.

1. The theoretical analysis has given significant insight into the stability characteristics of hingeless rotor blades primarily because it is simple enough to comprehend while still retaining the essential degrees of freedom. Instabilities were shown to be the result of aerodynamic and inertial coupling of the flap and lead-lag degrees of freedom.
2. For the basic flap-lag case, the least stable condition occurred when the lead-lag frequency was equal to the flap frequency and the flap frequency was $\sqrt{4/3}$. It was found that profile drag, structural damping, and aerodynamic induced drag were stabilizing.
3. An experimental investigation confirmed that the theoretically destabilizing effects of aerodynamic and inertial flap-lag coupling actually occurred in a real system. Nonlinearities resulting from blade stall at high collective pitch angles increased lead-lag damping. The theory was also able to account for these nonlinearities.
4. The inclusion of flap-lag elastic coupling and kinematic pitch-lag coupling were found to have an important influence on the rotor blade stability. The elastic coupling is structurally inherent in all hingeless rotor blades but has not previously been recognized as an important factor for stability. The present theoretical analysis indicates that the degree of elastic coupling, depending on the lead-lag frequency, determines whether the rotor blade will be stable or unstable. The degree of elastic coupling is also shown to be dependent on several rotor blade design parameters,

such as pitch bearing location and flexibility distributions.
5. In practical terms the present results are encouraging because they permit a much needed understanding of hingeless rotor blade stability and should provide the basis for a rational approach to the design of hingeless helicopter rotors. For instance, configurations providing a high degree of elastic coupling can significantly improve lead-lag damping and a judicious choice of pitch-lag coupling can also be very beneficial.

The present work has stimulated the continuation of this research and several areas are currently under study. Experimental verification of the high damping afforded by elastic coupling is presently underway while theoretical efforts are aimed at studying the important effects of the torsional degree of freedom.

REFERENCES

1. Ormiston, R. A. and Hodges, D. H.; "Linear Flap-Lag Dynamics of Hingeless Rotor Blades in Hover," Journal of the American Helicopter Society; Vol. 17, No. 2, April 1972.
2. Gessow, A. and Myers, G. D., Jr.; Aerodynamics of the Helicopter, Frederick Ungar Publishing Co., New York, 1967.
3. Jacobs, E. N. and Sherman, A.; "Airfoil Section Characteristics as Affected by Variations of the Reynolds Number," NACA Report No. 586, June 1936.

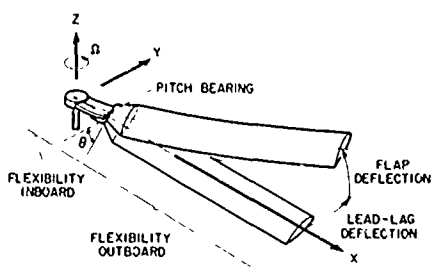

Figure 1. - Schematic representation of a hingeless rotor blade in rotating coordinate system, showing elastic bending deflections.

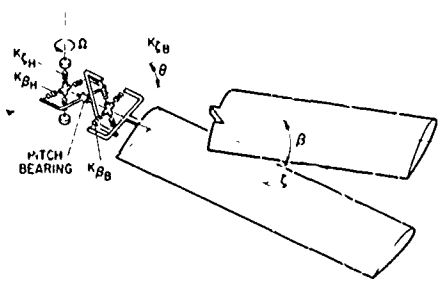

Figure 2. - Centrally-hinged, rigid blade representation with spring stiffness arranged inboard and outboard of the pitch bearing.

156.

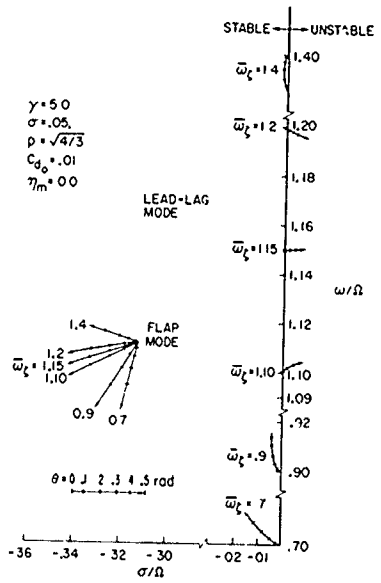

Figure 3. - Locus of roots with increasing pitch angle for basic flap-lag equations without elastic coupling, R = 0.0 .

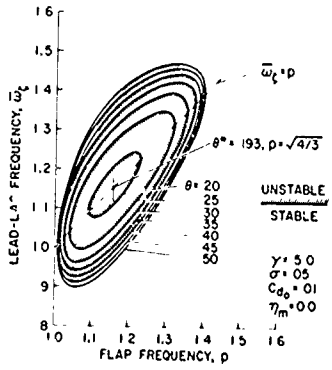

Figure 4. - Stability boundaries for basic flap-lag equations, R = 0.0 .

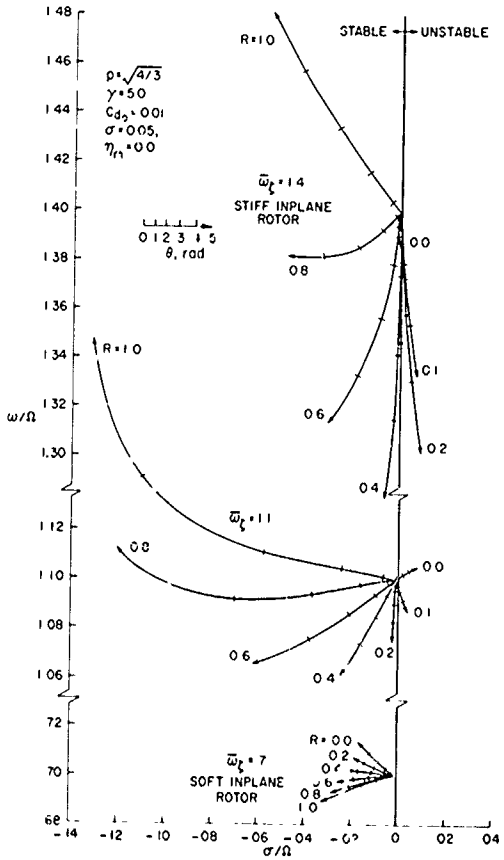

Figure 5. - Locus of lead-lag mode roots with increasing pitch angle for flap-lag equations with variable elastic coupling, R ≠ 0.0 .

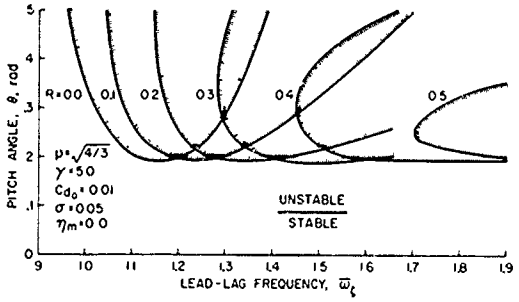

Figure 6. - Stability boundaries for flap-lag equations with variable elastic coupling, $R \neq 0.0$.

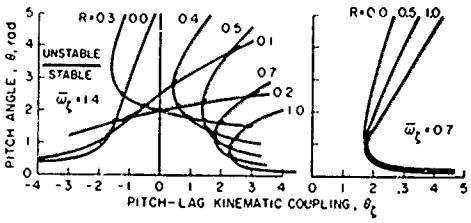

Figure 7. - Stability boundaries for flap-lag equations with variable elastic coupling and kinematic pitch-lag coupling.

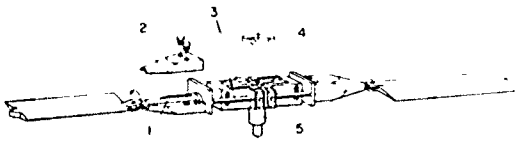

Figure 8. - Experimental rotor hub.

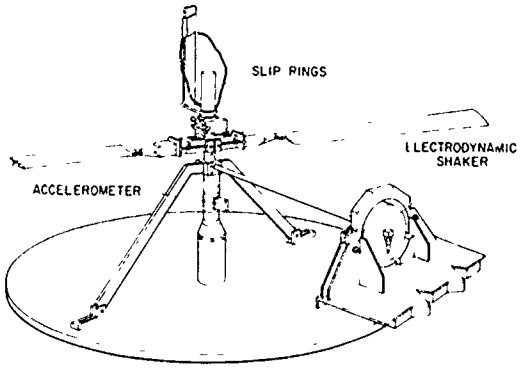

Figure 9. - Experimental rotor test set-up.

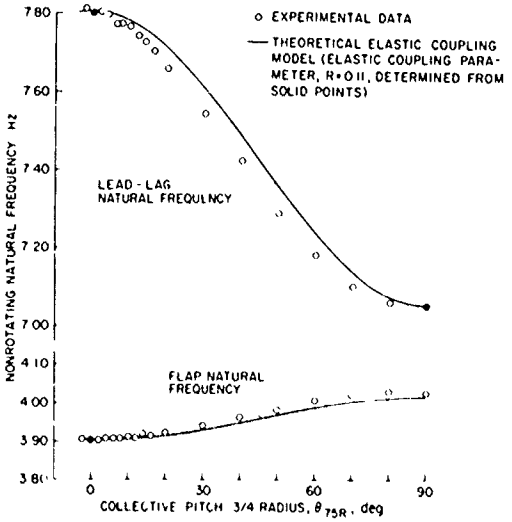

Figure 10. - Nonrotating flap and lead-lag natural frequency variation with collective pitch angle.

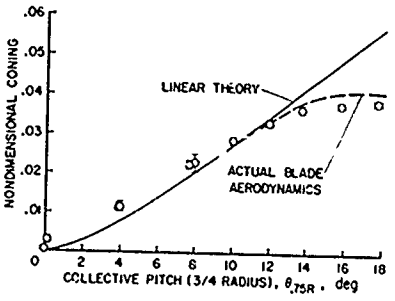

Figure 11. - Normalized blade coning angle variation with collective pitch angle.

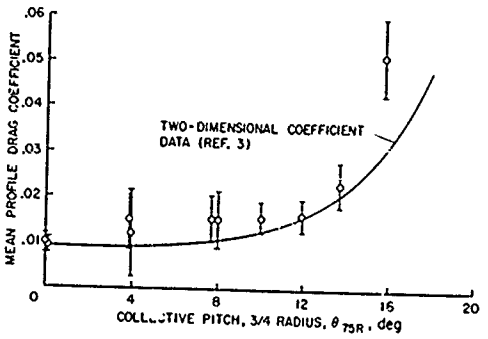

Figure 12. - Mean profile drag coefficient variation with collective pitch angle.

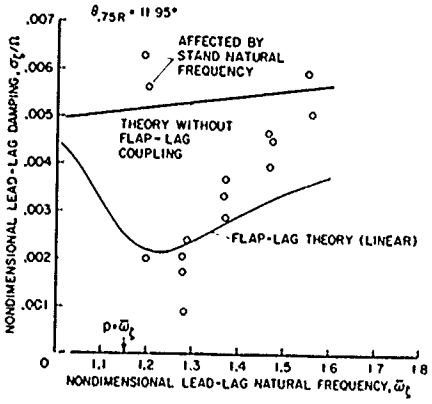

Figure 13. - Nondimensional lead-lag damping variation with blade nondimensional lead-lag natural frequency.

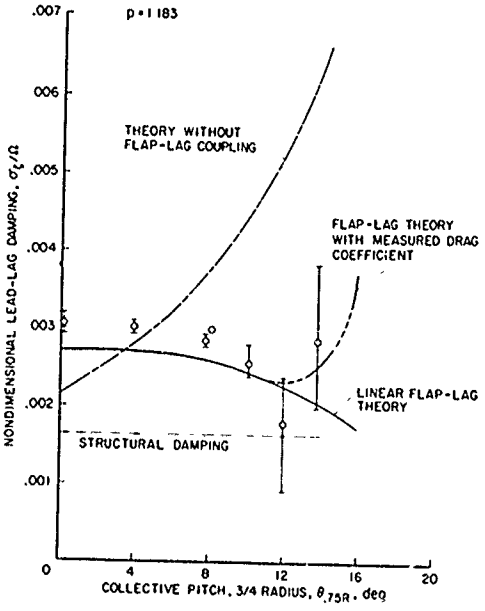

Figure 14. - Nondimensional lead-lag damping variation with collective pitch angle at $\bar{\omega}_\zeta$ = 1.278